Molecular Dynamics Study of Hydrated Faujasite-Type Zeolites

Katsuhiro Shirono,[†] Akira Endo,[‡] and Hirofumi Daiguji*,[†]

Institute of Environmental Studies, Graduate School of Frontier Sciences, The University of Tokyo, Tokyo 113-0033, Japan, and Research Institute for Innovation in Sustainable Chemistry, National Institute of Advanced Industrial Science and Technology (AIST), Tsukuba, Ibaraki 305-8565, Japan

Received: June 22, 2004

Molecular dynamics (MD) simulations of hydrated zeolite NaX (Si/Al = 1.0) and NaY (Si/Al = 2.0) were done at a temperature of 300 K. The calculation results show that the adsorption of water occurs via a three-step mechanism in zeolite NaX: (1) adsorption around Na, (2) formation of a monolayer on the walls, and (3) pore filling in the supercage during which adsorbed water molecules are localized around the 12-membered rings. Zeolite NaY adsorbs in a similar manner. However, at intermediate hydration states, cluster formation occurs around Na instead of monolayer formation. The calculated energy distribution functions suggest that in zeolite NaX, the water vapor adsorption can be expressed by using the Langmuir model with two adsorption sites, but in zeolite NaY, it is not Langmuir-type adsorption.

1. Introduction

Microporous and mesoporous materials have been applied as adsorbents.[1,2] Recently developed synthesis techniques allow the pore size to be controlled, making it possible to synthesize porous materials with various adsorption properties.[3,4] Knowledge of the structural and dynamical properties of adsorbates is essential for the design of adsorbents, but even in well-known crystals such as zeolites, the properties of adsorbates have not yet been clarified.

Zeolites are one of the most commonly used adsorbents,[5] and hydrophilic zeolites exhibit type I isotherms in the IUPAC classification,[6] also called Langmuir isotherms. The Langmuir isotherm usually means the monolayer adsorption on the surface, but pore filling also promotes the adsorption in the microporous materials because the total amounts of adsorbates inside the microporous materials are larger than those expected from the surface area.[7] Möise et al.[8] investigated the effect of pore filling on the adsorption of water into the zeolite BaX and BaY by calorimetric measurement and Dubinin−Radushkevich analysis of isotherms. They suggested that water is adsorbed in three different steps: (1) adsorption onto hydrophilic sites, (2) formation of a monolayer on the walls, and (3) pore filling in the supercages. Although there is much experimental data on calorimetric measurements, the onsets of monolayer formation and pore filling have not yet been clarified, and the effects of the type of exchangeable cations and of the Si/Al ratio on these processes are unresolved.

Molecular simulation is a useful tool to solve these problems. However, predictive calculations of adsorbates in microporous and mesoporous materials are still challenging. For molecular simulations on zeolites, many studies have been done so far,[9,10] and molecular simulation techniques have been applied to a range of zeolite/adsorbate systems.[11] In the case of zolite/water systems, a number of modeling studies about the interaction of water molecules with hydrophobic zeolites have been performed, and recent simulation strategies permit more realistic representation of the behavior of water. Bussai et al.[12,13] developed the silicalite-1/water potential function using quantum chemical calculations at the Hartree−Fock level using 6-31G* basis sets, and a series of MD simulations were performed to examine changes to the structural and dynamical properties of water molecules in silicalite-1 as a function of temperature and loadings. Cicu et al.[14] developed electric field-dependent potentials for flexible water molecules adsorbed in zeolites. This water model was able to reproduce the experimental trend of the influence of an electric field on the geometry and vibrational frequencies of water molecules. Demontis et al.[15] executed MD simulations of water in the hydrophobic silicalite with the same potentials. Smirnov et al.[16] employed a variable partial atomic charge model for water and performed MD calculations coupled with electronegativity method (EEM) calculations[17,18] on water in hydrophobic zeolites. These studies succeeded in reproducing the geometry and vibrational frequencies of water molecules adsorbed in zeolites. However, if the purpose of study is to understand the adsorption process in hydrophilic zeolites, it is important to clarify not only the behavior of water molecules at specific adsorption sites but also the description of structural distribution and diffusion of water in a range spanning from the dehydration to the hydration state. Faux[19] performed MD simulations of hydrated zeolite 4A for a range of hydration in which water dynamics in zeolite 4A was investigated in detail. The water molecules were assumed to interact via the SPC/E potential.[20] Though the calculated diffusion coefficient of water was approximately 3 times larger than the experimental one, the calculated adsorption heat was in good agreement with the experimental one.

For faujasite-type zeolites, Jaramillo and Auerbach[21] developed and validated a new force field for Na cations, which

* Corresponding author. E-mail: daiguji@k.u-tokyo.ac.jp. Tel: +81-3-5841-8587. Fax: +81-3-3818-0835.
[†] The University of Tokyo.
[‡] Research Institute for Innovation in Sustainable Chemistry, AIST.

10.1021/jp047293t CCC: $30.25
Published on Web 02/05/2005

TABLE 1: Reported and Calculated Partial Charges of Framework Atoms of Zeolite and Cations

	Lee et al.[a]	Demontis et al.[b]	Auerbach et al.[c]	Faux[d]	Jaramillo et al.[e] (q_{i0})		q_i (e)	$\lvert(q_i - q_{i0})/q_{i0}\rvert$
O	$-0.4431 \sim -0.4380$	-1.03	-1.2	-1.86875	-1.2[f] (-1.025[g])	O1	-1.130 ± 0.047	0.0583
						O2	-1.245 ± 0.005	0.0375
						O3	-1.244 ± 0.004	0.0367
						O4	-1.162 ± 0.039	0.0317
Si	0.6081	1.85	2.4	3.7	2.05		2.150 ± 0.026	0.0488
Al	0.6081	1.27	1.4	2.7775	1.75		1.631 ± 0.005	0.068
Na	0.55	1	1	1	1		1	

[a] Ref 24. [b] Ref 25. [c] Ref 26. [d] Ref 19. [e] Ref 21. [f] Oxygen bridging an Al atom and a Si atom. [g] Oxygen bridging two Si atoms.

explicitly distinguishes between Si and Al atoms, as well as different types of oxygen in the framework. This new force field gives excellent agreement with experimental data on cation position, site occupancy, and vibrational frequencies for most cations in zeolites NaX and NaY. For adsorbed water molecules in faujasite-type zeolites, in most studies the purpose was to clarify the position of water molecules at low hydration levels and to clarify the effect of adsorbed water molecules on the gas separation and catalytic reactions.[22,23] However, research to investigate the adsorption process in a range spanning from the dehydration to the hydration state in faujasite-type zeolites is limited. Such information is needed, however, to understand the adsorption process and to clarify the structural and dynamical properties of water molecules at intermediate hydration states. In addition, the effect of the Si/Al ratio on the adsorption process is still unresolved.

This paper reports the results of MD simulations of zeolites NaX and NaY for a range of hydration. The main purpose is to clarify the onset of monolayer formation and pore filling in supercages and the effect of the Si/Al ratio on these processes. This paper is organized as follows: Section 2 provides details of the MD simulation, including a discussion of the choice of potentials; Section 3 describes the calculation results. Section 4 provides a summary of the main results of our study.

2. Methodology

2.1. Charge Distribution in Zeolite Frameworks. For the framework of zeolite and cationic ions, several models have been proposed. In particular, there has been debate about the magnitude of the effective partial charge on the silicon, aluminum, and oxygen atoms. The charge distributions of several models[19,21,24−26] are summarized in Table 1. The charge distribution in zeolite frameworks is directly related to the Coulomb interactions between the water−zeolite framework. Therefore, to adopt the model expressing it accurately, the charge distribution of zeolite frameworks was calculated with EEM. The EEM is a semiempirical approach to density functional theory. It allows the direct calculation of average electronegativity and the charge distribution in a molecule or solid as follows:

$$\chi = \chi_i^* + 2\eta_i^* q_i + \sum_{i \neq j}^{n} q_j J_{ij} \qquad (1)$$

where χ(eVe^{-1}) is the electronegativity and χ_i^* (eVe^{-1}), η_i^* (eVe^{-2}), and q_i are the electronegativity, hardness, and charge of atom i, respectively. For a system with n atoms, a set of n of these equations is solved, along with an equation that constrains the net charge in the system. In this study, EEM calculation was done by using the method proposed by Njo et al.,[27] in which J_{ij} was calculated by using the simplified form proposed by Lowen and Vogt.[28] In EEM, one equalizes the electronegativities of atoms by requiring that

$$\begin{pmatrix} 2\eta_1^* & J_{12} & \cdots & J_{1n} & 1 \\ J_{21} & 2\eta_2^* & \cdots & J_{2n} & 1 \\ \vdots & \vdots & \ddots & \vdots & \vdots \\ J_{n1} & J_{n2} & \cdots & 2\eta_n^* & 1 \\ 1 & 1 & \cdots & 1 & 0 \end{pmatrix} \begin{pmatrix} q_1 \\ q_2 \\ \vdots \\ q_n \\ -\chi \end{pmatrix} = \begin{pmatrix} -\chi_1^* - q_{Na}\sum_i^{n_{Na}} J_{1i} \\ -\chi_2^* - q_{Na}\sum_i^{n_{Na}} J_{2i} \\ \vdots \\ -\chi_n^* - q_{Na}\sum_i^{n_{Na}} J_{ni} \\ -n_{Na}q_{Na} \end{pmatrix} \qquad (2)$$

where q_{Na} and n_{Na} are the charge of Na ions and the number of Na ions per unit cell, respectively. The values assumed in this study were $q_{Na} = +1.0e$. The parameters used for each kind of ion, $\{\chi_i^*\}$ $\{\eta_i^*\}$ $\{J_{ii}^0\}$, are from ref 27, except the value of J_{NaNa}^0, which was taken from ref 18, $J_{NaNa}^0 = 0.825$ (Å^{-1}). In this study, the charges of all ions except Na in the unit cell of dehydrate zeolite NaX ($Na_{96}Si_{96}Al_{96}O_{384}$) were calculated with EEM in the periodic boundary condition. Na ions were located at 64 sites in the center of the 6-membered rings and 32 sites around the 4-membered rings.[29] The calculation results are summarized in Table 1. The charges of oxygen atoms are averaged at each of four equivalent positions.[29] The partial charges calculated here are in good agreement with those proposed by Jaramillo and Auerbach.[21] They also proposed the cation−zeolite framework potential and reported the MD simulations of zeolites NaX and NaY incorporating with the zeolite framework potential proposed by Auerbach et al.[26] The model gives excellent agreement with experimental data on cation position, site occupancy, and vibrational frequencies for most cations in zeolites NaX and NaY. Therefore, in the following simulations, the partial charges and the cation−zeolite framework potential proposed by Jaramillo and Auerbach[21] and the zeolite framework potentials proposed by Auerbach et al.[26] were used.

2.2. Potential Functions between Water−Zeolite Framework and Water−Cation. The water molecules were assumed to interact via the SPC/E potential.[20] In this section, the potentials between the water−zeolite framework and water−cation were discussed. The potential between water−zeolite framework involved two contributions: a Coulomb interaction between all the atoms and a Born−Mayer−Huggins (BMH) interaction between the oxygen atoms of water (OW) and the framework oxygen atoms (OZ). The BMH potential function can be expressed as:

$$U(r_{ij}) = A_{ij} \exp\left(-\frac{r_{ij}}{\rho_{ij}}\right) - \frac{C_{ij}}{r_{ij}^6} \qquad (3)$$

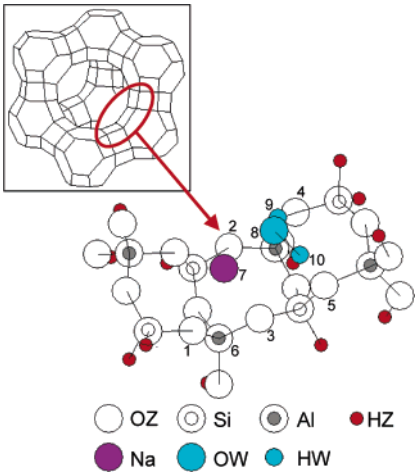

Figure 1. Molecular model around the four-membered ring of zeolite NaX and the optimized structure, including an adsorbed water molecule. OW, HW, and OZ represent oxygen and hydrogen atoms of water molecules and oxygen atoms of framework zeolite, respectively.

In the calculation of the BMH parameters between different types of atoms, the following combination rules were used:[30]

$$A_{ij} = f_0(b_i + b_j)\exp\left(\frac{a_i + a_j}{b_i + b_j}\right)$$
$$\rho_{ij} = b_i + b_j$$
$$C_{ij} = \sqrt{c_i c_j} \qquad (4)$$

where $f_0 = 1$ (kcal Å^{-1} mol^{-1}) $= 4.3384 \times 10^{-2}$ (eV Å^{-1}) is a conversion factor. The parameters a and b are the size and hardness of ions, respectively, with units of Å. The parameters for the framework oxygen atoms calculated by Auerbach et al.[26] were $a_{OZ} = 2.037$ Å, $b_{OZ} = 0.1797$ Å, and $c_{OZ} = 196.1$ eV. To apply these combination rules, the Lennard−Jones (LJ) potential function of the SPC/E water model was fitted to the BMH potential function expressed by using eq 3 in the range from 3.0 to 7.0 Å. The fitted parameters were $a_{OW} = 1.694$ Å, $b_{OW} = 0.1179$ Å, and $c_{OW} = 27.147$ eV. From eq 4, the BMH parameters between OW and OZ were determined to be $A_{OW-OZ} = 3599.405$ eV, $\rho_{OW-OZ} = 0.2976$ Å, and $C_{OW-OZ} = 72.965$ eV. The potential between water−Na ion also involved two contributions, a Coulomb interaction between all the atoms and a BMH interaction between OW and Na ions, and the BMH parameters between OW and Na ions are the same as those between OZ and Na ions: $A_{OZ-Na} = 5270.0$ eV, $\rho_{OZ-Na} = 0.2468$ Å, and $C_{OZ-Na} = 66.0$ eV.[21]

To validate the accuracy of these potential functions, the position of water molecules adsorbed at the four-membered rings was calculated by using density functional theory (DFT). The structure around the four-membered ring of zeolite NaX was modeled as shown in Figure 1. This system included four Al atoms in eight T-atoms. The overall charge of this system was determined to be $-3e$ assuming that all atoms were completely ionized. The calculations were done using Gaussian 98.[32] The B3LYP hybrid exchange-correlation functional and the 6-31G-(d) basis sets were used in this calculation. Figure 1 shows the optimized structure of this system calculated with DFT. The structure calculated with the Monte Carlo (MC) method using the potential functions mentioned above was almost the same. In the MC calculation, the partial charges of H atoms in SiH and AlOH were assumed to be $-0.4239e$ and $+0.4239e$, respectively. The absolute values of these charges are the same as q_{HW}, but we found that the calculation results depend marginally on these values. The distances between OW and sodium ions, OW and the nearest OZ, and HW and the nearest OZ calculated with DFT and MC are summarized in Table 2. These calculation results agree well with each other.

TABLE 2: Interatomic Distances Calculated with Density Functional Theory (DFT) and Monte-Carlo (MC) Methods[a]

pair of atoms	DFT	MC
OW(8)−Na(7)	2.282	2.294 ± 0.090
OW(8)−OZ(3)	3.432	3.402 ± 0.135
OW(8)−OZ(2)	3.734	3.687 ± 0.168
HW(10)−OZ(5)	1.800	1.949 ± 0.192
HW(9)−OZ(4)	1.943	2.054 ± 0.201
NA(7)−AL(6)	2.897	2.778 ± 0.083
NA(7)−OZ(3)	2.523	2.332 ± 0.088
NA(7)−OZ(1)	2.413	2.415 ± 0.111

[a] Atomic numbers are shown in Figure 1.

2.3. Calculation Conditions. MD simulations were done using NVT dynamics at 300 K by using the Nosé thermostat.[33,34] Periodic boundary conditions were used throughout. The Si/Al ratios of model zeolites NaX and NaY were 1 and 2, respectively. Water molecules were placed at random within the supercages to the desired concentration and allowed to equilibrate at 300 K for at least 100 ps. In all simulations, the time step was 1 fs and simulations were run for a total time of about 400 ps with atomic positions output every 0.2 ps. Simulations were performed with 0, 32, 64, 96, 128, 160, 192, and 224 water molecules in the simulation cell, the latter corresponding to approximately full hydration. The side length of the cell was 25.0099 Å for NaX and 24.8536 Å for NaY. These values were derived from X-ray diffraction measurements of zeolites NaX[29] and NaY[35] with almost the same Si/Al ratios. The positions of T-atoms were assumed to be those proposed by Loewenstein[36] and Dempsey et al.[37] All bond lengths of water molecules were rigidly constrained by using the SHAKE algorithm,[38] and electrostatic interactions were calculated with the Ewald method.[38]

3. Results and Discussion

3.1. Distribution of Sodium Ions. In the present MD simulations, Na ions at cation sites did not move appreciably during the entire simulation period in any hydration state. Therefore, it is important to determine realistic initial positions of Na ions. In this study, for zeolite NaX, 96 Na ions were distributed at SI′, SII, and SIII sites with 32 per site, and for zeolite NaY, 64 Na ions were at SI, SII, and SIII sites with 16, 32, and 16, respectively. For the surface of a supercage, which strongly affects the adsorption process, the difference in Na ion distribution between zeolites NaX and NaY is only the number of sodium ions at SIII sites. For the surface of sodalite cages, sodium ions located at SII sites keep their positions and prevent water molecules from penetrating into sodalite cages, either in zeolites NaX or NaY. The rest of the Na ions are located at the center of six-membered rings that are on the top and bottom surfaces of hexagonal prisms in zeolite NaX, and those in zeolite NaY are located at the center of hexagonal prisms. These Na ions do not significantly affect the adsorption process, because they are not on the outermost surface of a supercage but are located at the most symmetric positions. The occupancy of each site is not completely the same as that obtained experimentally or theoretically,[29,35,39−43] but this occupancy can express the qualitative features that the number of hydrophilic sites in zeolite NaX is larger than that in zeolite NaY and the average distance between hydrophilic sites in zeolite NaX is smaller than that in zeolite NaY.

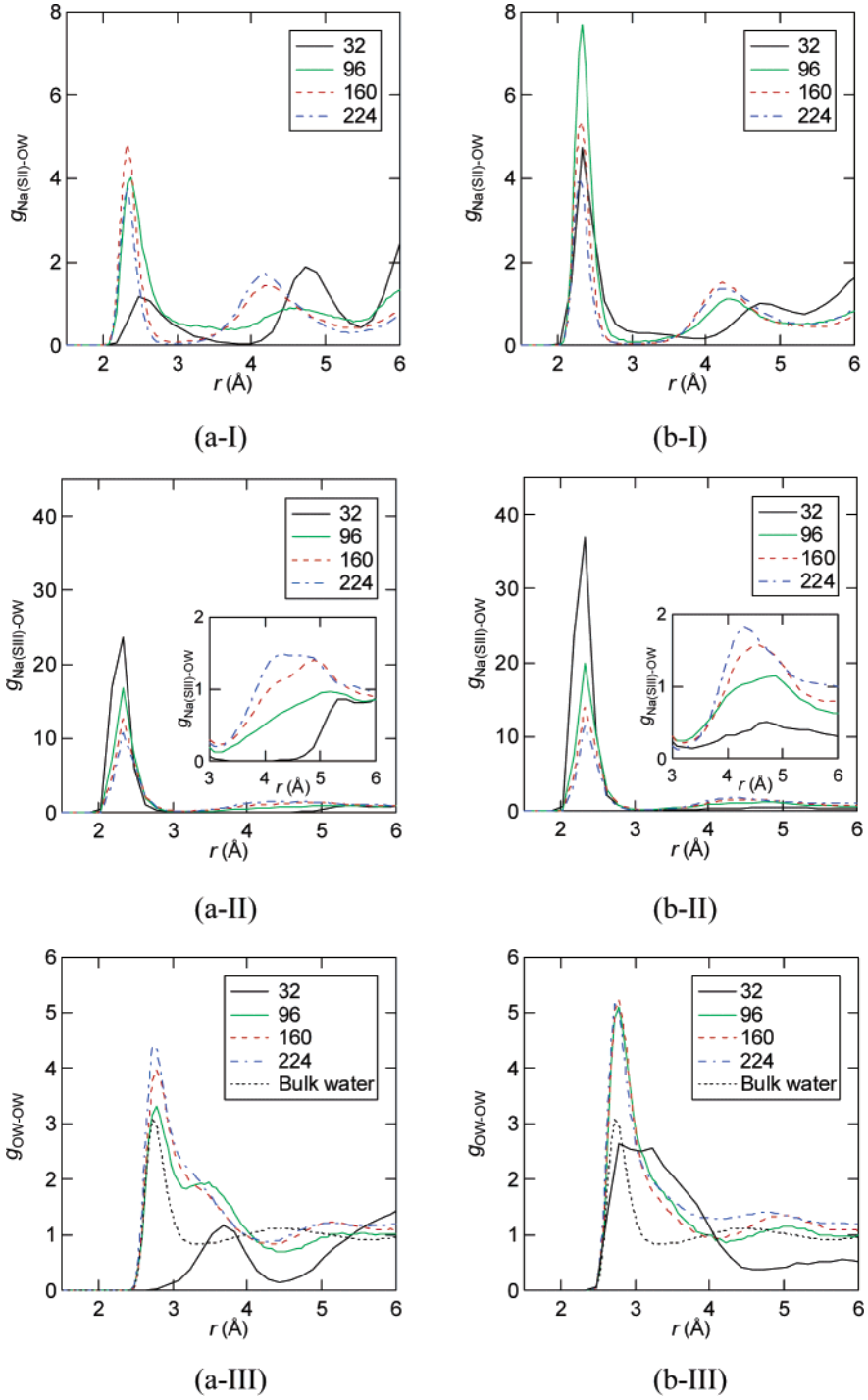

Figure 2. Radial distribution functions between (I) Na(SII)−OW, (II) Na(SIII)−OW and (III) OW−OW for zeolites (a) NaX and (b) NaY.

3.2. Distribution of Water Molecules. Figures 2a-I,II,III and 2b-I,II,III show the radial distribution functions between (I) Na(SII)−OW, (II) Na(SIII)−OW, and (III) OW−OW, $g_{Na(SII)-OW}$, $g_{Na(SIII)-OW}$, and g_{OW-OW}, for zeolites (a) NaX and (b) NaY, respectively. Because the first peaks of $g_{Na(SIII)-OW}$ are much larger than those of $g_{Na(SII)-OW}$ at low hydration both in zeolites NaX and NaY, water molecules are initially adsorbed around Na ions at the SIII site. For the second peak of $g_{Na(SIII)-OW}$, the position changes as the number of water molecules increases in zeolite NaX [inset in Figure 2a-II]; however, it does not change so much in zeolite NaY [inset in Figure 2b-II]. These results suggest that in zeolite NaX, because there are many hydrophilic sites, that is, the site around a Na ion at the SIII site as shown in Figure 1 and the site between two Na ions at the SII and SIII sites (linked SII−water−SIII structure in ref 39), water molecules do not appear in the second hydration shells around Na ions at the SIII site until high hydration; however, in zeolite NaY, because the number of hydrophilic sites is small, the water molecules form a cluster around Na ions at the SIII site and appear in the second hydration shells from low hydration. For the radial distribution functions between OW−OW, g_{OW-OW}, in zeolite NaX, the first peak is located at $r = 3.5$ Å at low hydration [Figure 2a-III]. This is just the intermolecular distance between water molecules at two neighboring hydrophilic sites, the site around a Na ion at the SIII site as shown in Figure 1 and the site between two Na ions at the SII and SIII sites. On the other hand, in zeolite NaY, the position of the first peak is the same as the intermolecular

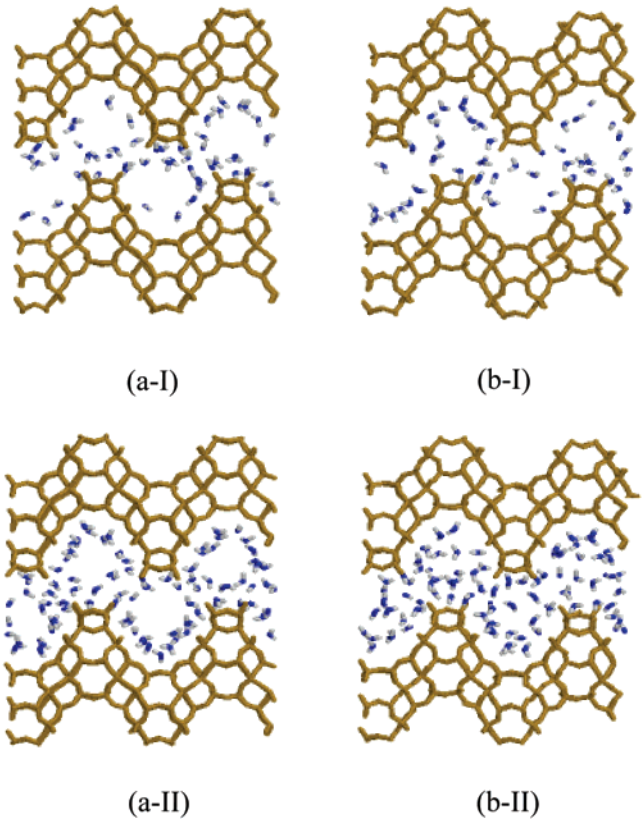

Figure 3. Snapshots of water distribution in a cross-section through interconnecting cavities in zeolites at different numbers of water molecules per unit cell: (I) $N = 128$ and (II) $N = 224$ for zeolites (a) NaX and (b) NaY, respectively. The figures show water molecules and zeolite frameworks. The water molecules were depicted only within the thickness of 7.0 Å.

distance of liquid water [Figure 2b-III]. These results also support the adsorption process mentioned above.

Figures 3a-I,II and 3bI,II show snapshots of water distribution in a cross-section through interconnecting cavities at different numbers of water molecules per unit cell: (I) $N = 128$ and (II) $N = 224$, for zeolites (a) NaX and (b) NaY, respectively. At intermediate hydration ($N = 128$), the water molecules are localized near the frameworks both in zeolites NaX and NaY [Figures 3a-I and 3b-I]. At high hydration ($N = 224$), in zeolite NaX [Figure 3a-II], water molecules are localized near the frameworks and around the junctions between neighboring supercages, that is, around the 12-membered rings [see inset in Figure 1]. On the other hand, in zeolite NaY [Figure 3b-II], water molecules are distributed in the whole area inside supercages.

3.3. Differential Heat of Adsorption. To evaluate the interaction energy, the differential heat of adsorption was investigated. The differential heat of adsorption, $|\partial H/\partial N|$, is defined as:

$$\left|\frac{\partial H}{\partial N}\right| = \left|\frac{\partial U}{\partial N} + RT\right| \tag{5}$$

where $\partial U/\partial N$ is the derivative of the potential energy with respect to the number of water molecules, and R and T are gas constant and temperature, respectively. The $\partial U/\partial N$ was calculated in two different ways. One way is to fit a polynomial function to the potential energy vs the number of water molecules ($U-N$) curve, and then to derive the polynomial function with respect to N. The other way is to calculate $(U^{N+\Delta N} - U^N)/\Delta N$, where U^N is the potential energy of a unit cell containing N water molecules and ΔN is the difference in N between two

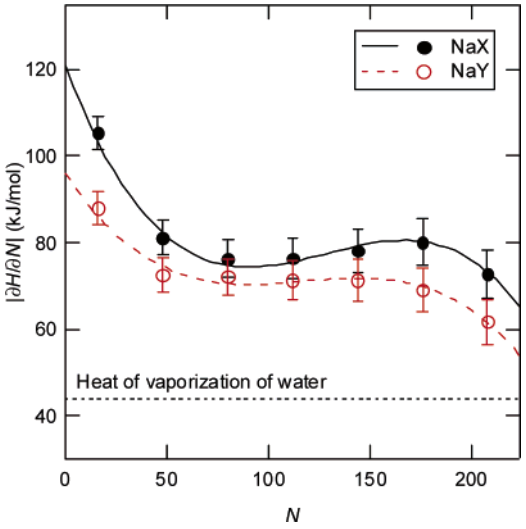

Figure 4. Differential heat of adsorption, $|\partial H/\partial N|$, for zeolites NaX and NaY. Lines and points were obtained from polynomial and linear interpolation, respectively. N is the number of water molecules per unit cell.

different hydration states. The differential heat of adsorption at $N + \Delta N/2$ was calculated as follows: $|\partial H/\partial N|^{N+\Delta N/2} = |(U^{N+\Delta N} - U^N)/\Delta N + RT|$. The calculated differential heats of adsorption are plotted in Figure 4. Although the calculated values are 10∼15 kJ/mol larger than the measured ones[44−46] in any hydration state, the trends agree. The discrepancy between calculated and measured energies is discussed in Section 3.5.

The potential energy of a unit cell, U, can be decomposed into three terms: the potential energies between water−zeolite, water−water, and zeolite−zeolite. The derivatives of the potential energy with respect to the number of water molecules, $\partial U/\partial N$, can also be decomposed as follows:

$$\frac{\partial U}{\partial N} = \frac{\partial U_{W-Z}}{\partial N} + \frac{\partial U_{W-W}}{\partial N} + \frac{\partial U_{Z-Z}}{\partial N} \tag{6}$$

Figures 5a and 5b show the differential heat adsorption and the negatives of three decomposed terms for zeolites NaX and NaY, respectively. For zeolite NaX, there are plateau regions in the $(-\partial U_{W-Z}/\partial N) - N$ and $(-\partial U_{W-W}/\partial N) - N$ curves, but for zeolite NaY, there are no plateau regions in these curves. These calculation results suggest that in zeolite NaX, water molecules are adsorbed at equivalent energy sites, but in zeolite NaY, water molecules are gradually adsorbed at higher energy sites with increasing N.

Figures 6a and 6b show the energy distribution functions between water and zeolite for zeolites NaX and NaY, respectively. For zeolite NaX, there are two peaks in the energy distribution functions. The interaction energy of the first peak, $u_{W-Z} = -130 \sim -110$ kJ/mol, corresponds to that when a water molecule is adsorbed around a Na ion at the SIII site as shown in Figure 1 or between two Na ions at the SII and SIII sites. The interaction energy of the second peak, $u_{W-Z} = -80 \sim -60$ kJ/mol, corresponds to that when a water molecule is adsorbed in the supercage except for the two positions mentioned above. At low hydration, $N = 32$, only the first peak appears. After the hydrophilic sites are fully occupied, the second peak appears. This adsorption process can be expressed by using the Langmuir model with two adsorption sites.[47] For zeolite NaY, the first peak is lower than that of zeolite NaX because the number of Na ions at the SIII site is only 16. The second peak is distributed broadly, and the energy of the peak position increases with an

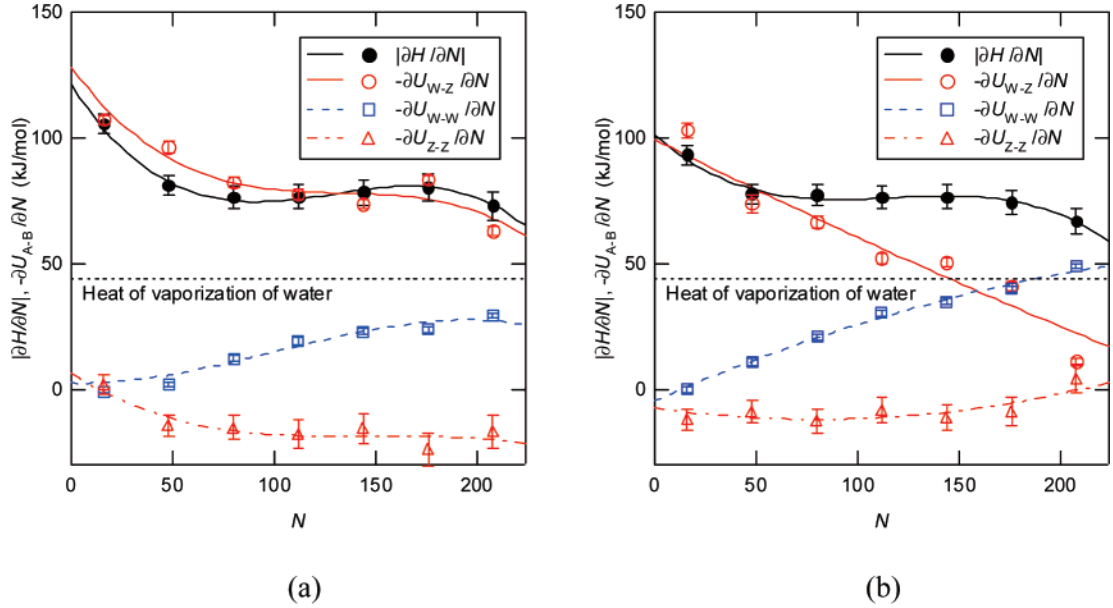

Figure 5. Differential heat of adsorption, $|\partial H/\partial N|$, and negatives of differential potential energies between water−zeolite, water−water, and zeolite−zeolite, $-\partial U_{W-Z}/\partial N$, $-\partial U_{W-W}/\partial N$, and $-\partial U_{Z-Z}/\partial N$ for zeolites (a) NaX and (b) NaY. Lines and points were obtained from polynomial and linear interpolation, respectively. N is the number of water molecules per unit cell. Relevancy of these values is expressed by $|\partial H/\partial N| = -\partial U_{W-Z}/\partial N - \partial U_{W-W}/\partial N - \partial U_{Z-Z}/\partial N - RT$. RT is 2.494 kJ/mol at 300 K.

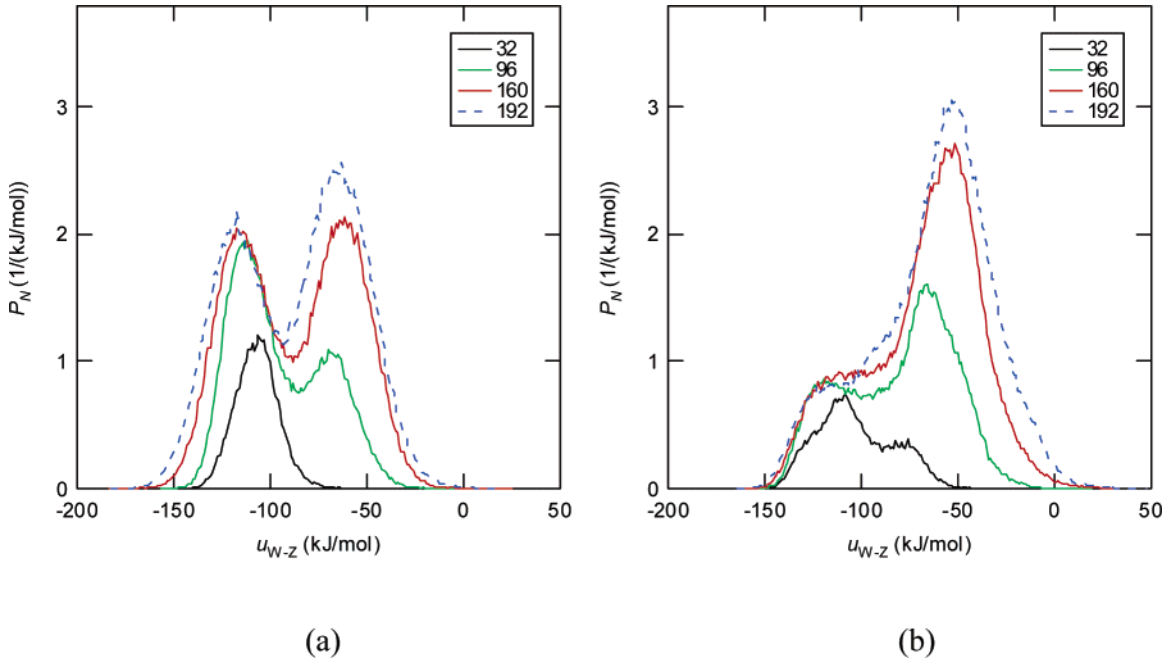

Figure 6. Energy distribution functions between water and zeolite for zeolites (a) NaX and (b) NaY. P_N is the number density per unit energy, 1/(kJ/mol). u_{W-Z} is the potential energy between water and zeolite, kJ/mol.

increasing the number of water molecules. This is not Langmuir-type adsorption.

3.4. Diffusion Coefficient. To evaluate the dynamical properties of water molecules inside zeolites NaX and NaY, the diffusion coefficients were calculated with mean square displacements (MSD). Figure 7 shows the computed diffusion coefficients as a function of the number of water molecules per unit cell, N. In any hydration state, the plot of MSD vs time shows a reasonably straight line with a well-defined gradient for the entire simulation time. The diffusion coefficient at $N = 160$ for zeolite NaX calculated here is 1.36×10^{-10} m^2/s, and the corresponding experimental value from ref 44 is $(1-2) \times 10^{-10}$ m^2/s; these values are in good agreement. However, at low hydration, because the calculated diffusion coefficient at $N = 32$ for zeolite NaX is 7.27×10^{-12} m^2/s, the distance water molecules diffuse for 400 ps is about 1 Å, which is much smaller than the center-to-center distance between neighboring supercages of of 10.83 Å. The diffusion coefficient calculated here represents the translational motion within the time scale of the simulation, but one should be cautious as to whether it represents a macroscopic measurement of diffusion coefficient, that is, long-range intercage diffusion of water. For zeolite NaX, the computed diffusion coefficient increases from 7.27×10^{-12} to 1.38×10^{-10} m^2/s with increasing the number of water molecules from 32 to 96. But as the number of water molecules increases further, the computed diffusion coefficient decreases. The trend of the curves of diffusion coefficient vs the number of water molecules agrees with that obtained from MD simula-

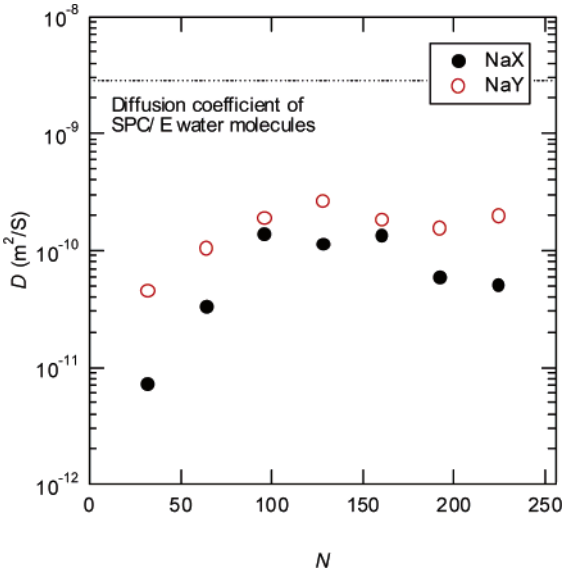

Figure 7. Diffusion coefficients of oxygen atoms of water molecules, *D*, in zeolites NaX and NaY as a function of the number of water molecules per unit cell, *N*.

tions on hydrated zeolite 4A by Faux,[19] in which the diffusion coefficient increases from 2.7×10^{-10} to 6.8×10^{-10} m^2/s with increasing the number of water molecules from 56 to 168 but decreases in the higher hydration state. This trend can also be observed in other types of hydrophilic zeolites.[48] For zeolite NaY, a similar trend can be observed, but the diffusion coefficients are slightly larger than those of zeolite NaX.

3.5. Molecular Model for MD Simulation. In the present molecular model, the calculation results of the differential heat of adsorption and the diffusion coefficient of water in zeolites NaX and NaY agree with the experimental ones qualitatively. However, because the calculated differential heats of adsorption are about 10% larger than the measured ones,[44−46] the interaction energy between water and zeolite may be slightly larger than the real values. There are two ways to improve the accuracy of calculating the interaction energy functions between water and zeolite: improvement of the accuracy of the non-Coulomb and Coulomb interaction energy functions. For non-Coulomb interactions, the simple combination rule expressed by eq 4 was used in the present study, but the non-Coulomb interaction energy function should be optimized for better agreement with experimental results such as the differential heat of adsorption and diffusion coefficient. For Coulomb interactions, the SPC/E liquid water model was used in the present study; however, Demontis et al.[15] reported that the calculated adsorption heat of water in hydrophobic zeolite is in good agreement with experimental values when the gas-phase polarization of water molecules was used. In addition, the partial charges of all atoms in water and in zeolites were fixed in this study; however, Smirnov et al.[16] employed a variable partial atomic charge model for water and performed MD calculations coupled with EEM calculations, in which EEM calculations were done at each time step of MD calculation to determine the partial atomic charges, on water in hydrophobic zeolites and reported that the dipole moment of water molecules in zeolites was smaller than that in bulk water. To improve the accuracy of the molecular model, not only optimization of the non-Coulomb interactions but also further investigation of the partial charges of all atoms is needed, including the development of variable partial charge models.

4. Conclusion

MD simulations of hydrated zeolite NaX (Si/Al = 1.0) and NaY (Si/Al = 2.0) were done at 300 K. We summarize the findings of our study as follows.

1. The differential heats of adsorption were well reproduced for zeolites NaX and NaY. The calculated results show that the adsorption of water occurs via a three-step mechanism in zeolite NaX: (1) adsorption around Na, (2) formation of a monolayer on the walls, and (3) pore filling inside the supercage during which water molecules are localized around the 12-membered rings. Zeolite NaY adsorbs in a similar manner. However, at intermediate hydration states, cluster formation occurs around Na instead of monolayer formation.

2. The calculated energy distribution functions suggest that in zeolite NaX, the water vapor adsorption can be expressed by using the Langmuir model with two adsorption sites, but in zeolite NaY, it is not Langmuir-type adsorption.

3. For zeolite NaX, the diffusion coefficient increases with increasing the number of water molecules. However, the diffusion coefficient decreases in the high hydration state.

4. In the present molecular model, the calculation results of the differential heat of adsorption and the diffusion coefficient of water in zeolites NaX and NaY agree with the experimental ones qualitatively. To improve of the accuracy of the molecular model, not only optimization of the non-Coulomb interactions but also further investigation of the partial charges of all atoms is needed, including the development of variable partial charge models.

References and Notes

(1) Moller, K.; Bein, T. *Chem. Mater.* **1998**, *10*, 2950.
(2) Morishige, M.; Fujii, H.; Uga, M.; Kimukawa, D. *Langmuir* **1997**, *13*, 3494.
(3) Thommes, M.; Köhn, R.; Fröba, M. *Appl. Surf. Sci.* **2002**, *196*, 239.
(4) Enke, D.; Janowski, F.; Schwieger, W. *Microporous Mesoporous Mater.* **2003**, *60*, 19.
(5) Derouane, E. G. *J. Mol. Catal. A: Chem.* **1998**, *134*, 29.
(6) Sing, K. S. W.; Everett, D. H.; Havic, R. A. W.; Moscou, L.; Pierotti, R. A.; Rouquerol, J.; Siemieniewska, T. *Pure Appl. Chem.* **1985**, *57*, 603.
(7) Dąbrowski, A. *Adv. Colloid Interfac.* **2001**, *93*, 135.
(8) Moïse, J. C.; Bellat, J. P.; Méthivier, A. *Microporous Mesoporous. Mater.* **2001**, *43*, 91.
(9) Auerbach, S. M. *Int. Rev. Phys. Chem.* **2000**, *19*, 155.
(10) Fuch, A. H.; Cheetham, A. K. *J. Phys. Chem. B* **2001**, *105*, 7375.
(11) Demontis, P.; Suffritti, G. B. *Chem. Rev.* **1997**, *97*, 2845.
(12) Bussai, C.; Hannongbua, S.; Fritzsche, S.; Haberlandt, R. *Chem. Phys. Lett.* **2002**, *354*, 310.
(13) Bussai, C.; Fritzsche, S.; Haberlandt, R.; Hannongbua, S. *J. Phys. Chem. B* **2003**, *107*, 12444.
(14) Cicu, P.; Demontis, P.; Spanu, S.; Suffritti, G. B.; Tilocca, A. *J. Chem. Phys.* **2000**, *112*, 8267.
(15) Demontis, P.; Stara, G.; Suffritti, G. B. *J. Phys. Chem. B* **2003**, *107*, 4426.
(16) Smirnov, K. S.; Bougeard, D. *Chem. Phys.* **2003**, *292*, 53.
(17) Mortier, W. J.; Ghosh, S. K.; Shankar, S. *J. Chem. Phys.* **1986**, *108*, 4315.
(18) Rappe, A. K.; Goddard, W. A., III. *J. Phys. Chem.* **1991**, *95*, 3358.
(19) Faux, D. A. *J. Phys. Chem. B* **1999**, *103*, 7803.
(20) Brendsen, H. J. C.; Grigera, J. R.; Straatsma, T. P. *J. Phys. Chem.* **1987**, *91*, 6269.
(21) Jaramillo, E.; Auerbach, S. M. *J. Phys. Chem. B* **1999**, *103*, 9586.
(22) Limtrakul, J.; Treesukol, P.; Ebner, C.; Sansone, R.; Probst, M. *Chem. Phys.* **1997**, *215*, 77.
(23) Svelle, S.; Arstad, B.; Koboe, S.; Swang, O. *J. Phys. Chem. B* **2003**, *107*, 9281.
(24) Lee, S. H.; Moon, G. K.; Choi, S. G.; Kim, H. S. *J. Phys. Chem.* **1994**, *98*, 1561.
(25) Demontis, P.; Suffritti, G. B.; Bordiga, S.; Buzzoni, R. *J. Chem. Soc., Faraday. Trans.* **1995**, *91*, 525.
(26) Auerbach, S. M.; Henson, N. J.; Cheetham, A. K.; Metiu, H. I. *J. Phys. Chem.* **1995**, *99*, 10600.
(27) Njo, S. L.; Fan, J.; Graaf, B. *J. Mol. Catal. A* **1998**, *79*, 134.

(28) Louwen, J. J.; Vogt, E. T. C. *J. Mol. Catal. A* **1998**, *134*, 63.
(29) Olson, D. H. *Zeolite* **1995**, *15*, 439.
(30) Sato, H.; Yamagishi, A.; Kawamura, K. *J. Phys. Chem. B* **2001**, *105*, 7990.
(31) Soper, A. K. *Chem. Phys.* **2000**, *258*, *121*. ISIS Disordered Materials Database. http://www.isis.rl.ac.uk/disordered/database.
(32) Frisch, M. J.; Trucks, G. W.; Schlegel, H. B.; Scuseria, G. E.; Robb, M. A.; Cheeseman, J. R.; Zakrzewski, V. G.; Montgomery, J. A., Jr.; Stratmann, R. E.; Burant, J. C.; Dapprich, S.; Millam, J. M.; Daniels, A. D.; Kudin, K. N.; Strain, M. C.; Farkas, O.; Tomasi, J.; Barone, V.; Cossi, M.; Cammi, R.; Mennucci, B.; Pomelli, C.; Adamo, C.; Clifford, S.; Ochterski, J.; Petersson, G. A.; Ayala, P. Y.; Cui, Q.; Morokuma, K.; Malick, D. K.; Rabuck, A. D.; Raghavachari, K.; Foresman, J. B.; Cioslowski, J.; Ortiz, J. V.; Stefanov, B. B.; Liu, G.; Liashenko, A.; Piskorz, P.; Komaromi, I.; Gomperts, R.; Martin, R. L.; Fox, D. J.; Keith, T.; Al-Laham, M. A.; Peng, C. Y.; Nanayakkara, A.; Gonzalez, C.; Challacombe, M.; Gill, P. M. W.; Johnson, B. G.; Chen, W.; Wong, M. W.; Andres, J. L.; Head-Gordon, M.; Replogle, E. S.; Pople, J. A. *Gaussian 98*, revision A.11; Gaussian, Inc.: Pittsburgh, PA, 1998.
(33) Nosé, S. *Mol. Phys.* **1984**, *52*, 255.
(34) Nosé, S. *J. Chem. Phys.* **1984**, *81*, 511.
(35) Fitch, A. N.; Jobic, H.; Renouprez, A. *J. Phys. Chem.* **1986**, *90*, 1311.
(36) Loewenstein, W. *Am. Mineral.* **1954**, *39*, 92.
(37) Dempsey, E.; Kühl, G. H.; Olson, D. H. *J. Phys. Chem.* **1969**, *73*, 387.
(38) Allen, M. P.; Tildesley, D. J. *Computer Simulation of Liquids*; Clarendon Press: Oxford, 1987.
(39) Kirschhock, C.; Hunger, B.; Martens, J.; Jacobs, P. A. *J. Phys. Chem. B* **2000**, *104*, 439.
(40) Olson, D. H. *J. Phys. Chem.* **1970**, *74*, 2758.
(41) Norby, P.; Poshni, F. I.; Gualtieri, A. F.; Hanson, J. C.; Grey, C. P. *J. Phys. Chem. B* **1998**, *102*, 839.
(42) Buttefey, S.; Boutin, A.; Mellot-Draznieks, C.; Fuchs, A. H. J. *J. Phys. Chem. B* **2001**, *105*, 9569.
(43) Beuvais, C.; Guerrault, X.; Coudert, F.; Boutin, A.; Fuchs, A. H. J. *J. Phys. Chem. B* **2004**, *108*, 399.
(44) Kirmse, A.; Kärger, J.; Stallmach, F.; Hunger, B. *Appl. Catal. A* **1999**, *188*, 241.
(45) Chuikina, V. K.; Kiselev, A. V.; Mineyeva, L. V.; Muttik, G. G. *J. Chem. Soc., Faraday Trans. 1* **1976**, *72*, 1345.
(46) Boddenberg, B.; Rakhmatkarieb, G. U.; Hufnagel, S.; Salimov, Z. *Phys. Chem. Chem. Phys.* **2002**, *4*, 4172.
(47) Langmuir, I. *J. Am. Chem. Soc.* **1918**, *40*, 1416.
(48) Paoli, H.; Méthivier, A.; Jobic, H.; Krause, C.; Pfeifer, H.; Stallmach, F.; Kärger, J. *Microporous Mesoporous. Mater.* **2002**, *55*, 147.